Greatly Enhanced Soot Scattering in Flickering CH_4 / Air Diffusion Flames

KERMIT C. SMYTH, JOEL E. HARRINGTON,* ERIK L. JOHNSSON, and WILLIAM M. PITTS

Building and Fire Research Laboratory, National Institute of Standards and Technology, Gaithersburg, MD 20899

Planar images of laser-induced fluorescence from OH · radicals and elastic scattering from soot particles are presented in time-varying, laminar CH_4/air diffusion flames burning in a co-flowing, axisymmetric configuration at atmospheric pressure. Acoustic forcing is used to phase lock the periodic flame flicker to the pulsed laser system operating at 10.13 Hz. For conditions where the tip of the flame is clipped, the intensity of the light scattered by the soot particles increases dramatically (by more than a factor of 7 for the maximum signals at a point) compared to a steady-state, laminar flame with the same mean fuel flow velocity. Comparison of the scattering signals integrated along the flame radius is carried out in the steady-state and time-varying flames as a function of height above the burner. Time-varying flames exhibit a larger range of combustion conditions than observed in corresponding steady-state flames, including different residence times, temperature histories, local stoichiometries, and strain and scalar dissipation rates. Thus, their investigation promises to yield new insights into a wide variety of chemistry-flowfield interactions which are prominent in turbulent combustion.

INTRODUCTION

Combustion involves complex interactions among high-temperature chemical reactions, fluid mixing processes, and the production of gaseous fuel components via both thermal and chemical degradation. Although our knowledge of fuel production pathways and rates is in its infancy for the general case of condensed-phase fuel decomposition, significant progress has been achieved in identifying the key gas-phase chemical reactions and the associated fluid mechanical mixing phenomena which occur under high-temperature combustion conditions. As a consequence, increasing attention is now focused on elucidating the strong coupling which occurs between chemical heat release and turbulent mixing, that is, chemistry-turbulence interactions.

Soot formation is an important process which is especially sensitive to the local combustion conditions, since the pre-particle soot inception chemistry is relatively slow [1]. In co-flowing, steady-state laminar diffusion flames the earliest soot particles are formed near the high-temperature, primary reaction zone and are then typically transported into richer and cooler regions by convection (buoyancy leads to increased air entrainment) and thermophoretic forces [2]. As a result, soot inception, growth, and oxidation occur sequentially [3]. This situation has simplified the analysis of scattering and extinction measurements in hydrocarbon flames. There now exist sufficient experimental data obtained in steady-state, laminar diffusion flames to characterize each of the major stages of soot production and destruction.

In recent years several new attempts have been made to utilize the extensive experimental data currently available to develop integrated models of soot formation and evolution. These studies include work by Moss et al. [4–6], Kennedy et al. [7, 8], Lindstedt et al. [9, 10], and Kent and Honnery [11–13]. In addition, Faeth et al. have constructed state relationships for soot concentrations in ethylene, acetylene, propane, and propylene diffusion flames [14–17]. Although the various modeling approaches differ a good deal, there are several common threads. The local temperature, mixture fraction, and residence time have been identified as important variables in soot production, in addition to the chemical structure of the fuel. Each of the modeling groups cited above has reported at least one successful

* National Research Council NIST Postdoctoral Research Associate, 1992–present.

Published 1993 by Elsevier Science Publishing Co., Inc. 0010-2180/93/$6.00

comparison between experimental measurements and calculated results for a limited set of laminar combustion conditions. However, in more complex flowfields many additional possible residence times, temperature histories, and local stoichiometries may exist for soot production and destruction, as well as a wider variation of strain and scalar dissipation rates. One might anticipate that chemistry-flowfield interactions will have a dramatic impact upon soot formation.

New planar imaging measurements of OH· laser-induced fluorescence and elastic scattering from soot particles are reported here in time-varying CH_4/air diffusion flames. The flowfield in these low-velocity flames is controlled by buoyancy, and in our experiments the methane fuel flow is perturbed acoustically and phase locked to a laser system operating at 10.13 Hz. The flames exhibit highly reproducible structure and a much wider range of local strain and scalar dissipation rates than a simple co-flowing, steady-state laminar flame. For example, under conditions where the flame tip is clipped, higher velocity and concentration gradients are evident than for the steady-state flames. The forced flames qualitatively illustrate the same dynamic phenomena as observed for unforced conditions in a broad range of low-speed diffusion flames which are subject to flickering instabilities. Thus, they can provide new information on the interaction of chemical processes and time-varying flowfields.

Methane has been chosen as the fuel for several reasons. Numerous species profile measurements have been made in our laboratory on steady-state, laminar CH_4/air diffusion flames using optical and mass spectrometric methods [18–24]. These results have been compared to detailed flame structure computations of Smooke [25]. In addition, recent imaging measurements of OH· laser-induced fluorescence and soot scattering have been made in the oxidation regions of steady-state, axisymmetric methane–air and ethylene–air diffusion flames [26]. The analysis of these results provides a useful guide for the interpretation of the images obtained in the time-varying flames. Methane–air flames are also the most often used in current attempts to include realistic chemistry in turbulent flows with either flamelet libraries or reduced chemical mechanisms [27].

TIME-VARYING, LAMINAR CH_4 / AIR DIFFUSION FLAMES

Diffusion flames burning gases, liquids, and even solid fuels often exhibit a natural flame flicker which arises from a buoyancy-induced flow instability [28]. Peak velocities occur in regions where the heat release is strongest, with the result that large outer vortex structures develop due to the shear between the hot gases and the slower moving, cooler co-flow. This vortex production has been described as a modified Kelvin–Helmholtz type of hydrodynamic instability induced by buoyancy [29, 30]. The vortices rotate from the high- to the low-velocity side of the flow. When the rotational vortex velocity is sufficiently large, the flame sheets are pulled towards the centerline and the flame tip is pinched off. In an axisymmetric geometry the frequency of this flame flicker, or tip clipping, correlates well with the fuel tube diameter, D, as $f \approx 1.5/(D)^{1/2}$, where D is given in meters [28, 31, 32]. For example, the natural flame flicker frequency for a 1-cm-diameter tube is expected to be close to 15 Hz. The fuel flow velocity at which flame flicker appears is found to depend upon the velocity of the air co-flow [33, 34], with higher co-flow velocities inhibiting the formation of the outer vortex structures and displacing them further downstream.

The study of flickering phenomena in low velocity, hydrocarbon diffusion flames dates back to at least 1928 [35] and has been pursued by numerous researchers using a wide variety of flow visualization and imaging techniques [28–59]. Both unforced and forced conditions have been investigated in these buoyancy dominated flames. Recent imaging experiments have been performed principally by three groups. Cantwell and colleagues [47, 48, 50, 51; see also 49] have superimposed luminous soot and schlieren images in CH_4/air flames. In one instance particle tracking velocity measurements were also combined with scattering from TiO_2 particles and OH· laser-induced fluorescence [48]. Chen, Roquemore, and coworkers [52–57] have combined TiO_2 scatter-

ing and thin-filament pyrometry temperature measurements to probe the dynamics of nitrogen-diluted propane–air flames. By varying the initial fuel flow velocity, a range of time-varying laminar, transitional, and turbulent flames has been studied. Pearson et al. [34, 58, 59] have used schlieren and NO_2 fluorescence imaging methods in methane and propane flames. In addition to these investigations, Dobbins and Subramaniasivam have employed thermophoretic sampling to characterize soot formation processes in unsteady flames of methane, ethylene, and acetylene [60].

Acoustic forcing of the fuel and air flows has also been used to investigate momentum dominated combustion conditions. Recent studies include those of Gutmark et al., who have utilized OH· imaging of an annular propane–air diffusion flame to follow the evolution and interaction of vortices and to estimate local temperatures [61–64]. Lovett and Turns have used velocity and temperature measurements as well as several flow visualization methods to characterize the effects of pulsing on propane jets [65, 66]. Kim et al. have investigated mixing near the nozzle of an acoustically forced propane–air flame by combining velocity measurements with schlieren and TiO_2 imaging [67]. In addition to the work on diffusion flames, vortex–chemistry interactions have been investigated in premixed CH_4/air flames by Cattolica and Vosen [68, 69], Jarosinski et al. [70], and Roberts et al. [71]. Laser-induced fluorescence imaging of OH· has been successfully employed to monitor the location of the primary, high-temperature reaction zone in several of these studies [68, 69, 71].

EXPERIMENTAL FACILITY FOR TIME-VARYING, LAMINAR DIFFUSION FLAMES

A new experimental facility has been developed at NIST to study time-varying, hydrocarbon diffusion flames using optical imaging methods. Unconfined, axisymmetric, laminar flames have been established at atmospheric pressure on a coannular burner, which consists of a 1.11-cm-diameter fuel tube surrounded by a 10.2-cm-diameter air annulus [72]. The air chamber is filled with glass beads followed by several fine mesh screens and a 2.54-cm-thick ceramic honeycomb section with 0.15-cm-square cells to provide a uniform air flow velocity. No beads or screens have been used for flow conditioning in the 13.7 cm long fuel tube, which is attached to a plenum and extends 0.4 cm above the honeycomb. The methane fuel cold flow velocity was 7.9 cm/s, and the co-flow air velocity was 10.4 cm/s.

The flame has been acoustically forced using sine-wave excitation of a loudspeaker attached to the plenum and phase locked to our pulsed dye laser system operating at 10.13 Hz. Figure 1 shows a schematic diagram of the experimental setup. A signal generator is used to create the variable amplitude sine-wave voltage, while a variable-delay pulse generator controls the phase of this imposed sine-wave voltage relative to the laser pulse. This arrangement allows interrogation of the flame dynamics as a function of height, forcing phase angle, and forcing amplitude. Although the phase locking has

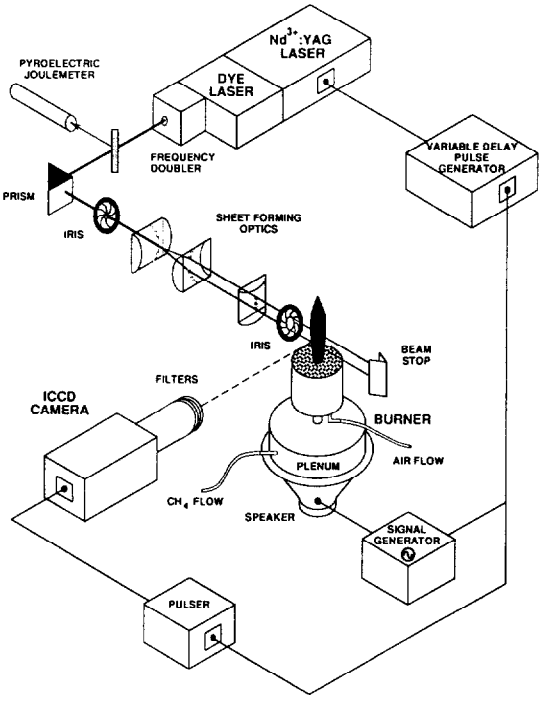

Fig. 1. Experimental setup for two-dimensional imaging of axisymmetric CH_4/air diffusion flames which are acoustically excited and phase locked to the pulsed dye laser system operating at 10.13 Hz. The polarization of the UV light can be varied using a Babinet–Soleil compensator (not shown).

been found to generate highly reproducible time-varying flames, some shot-to-shot wavering occurs in the images of the upper flame regions due to room drafts. For several of the images presented here, minor left–right corrections have been made in order to compensate for this flame wavering.

Our attempts to measure the peak-to-peak variation of the cold fuel velocity which occurs upon acoustic excitation have not been successful. Whereas a bubble flow meter attached to the fuel tube indicated a perturbation of only 3% for a 1 V (peak-to-peak voltage) excitation on the loudspeaker, a hot-wire anemometer gave 20–40 times higher values. Due to buoyancy effects at low velocities [73, 74], the hot-wire measurements were made for mean methane flow velocities in the 15–57 cm/s range and could not be obtained at the 7.9-cm/s velocity used in the imaging experiments. Phase-locked velocity measurements which employ seeding methods would be more definitive. At the downstream locations where flame clipping occurs, typically 20–50 mm above the fuel tube exit, buoyancy effects are expected to strongly increase the axial velocity in these time-varying flames. For example, in a steady-state ethylene–air diffusion flame using the same burner with initial fuel and air cold flow velocities of 4.0 and 8.9 cm/s, respectively, the axial velocity exceeds 100 cm/s at a height of only 20 mm for all radial positions $\leq$ 6 mm from the burner centerline [2].

The output from a Nd^{3+}:YAG pumped dye laser was frequency doubled to produce the UV beam, which was formed into a vertical sheet and focused into the flame with cylindrical lenses. Using a Babinet–Soleil compensator, the polarization of the light could be varied continuously from horizontal to vertical with respect to the detection axis. Laser-induced fluorescence from OH· and elastic light scattering signals from soot particles were observed with a Princeton Instruments CCD[1] camera equipped with a Nikon UV lens (f/4.5, 105 mm) and located at 90° to the propagation direction of the laser beam. This CCD camera incorporates a cooled detector chip with a 576 (row) × 384 (column) pixel format and an 18-mm microchannel plate image intensifier to provide gating and signal amplification.

The laser wavelength was tuned to 283.55 nm, corresponding to excitation of the $Q_1(8)$ line of the $A^2\Sigma^+ \leftarrow X^2\Pi_i$ (1,0) band of OH·. Excitation from the $N'' = 8$ level was selected in order to minimize the Boltzmann population correction for temperature variations (less than 5% over the range 1400 to 2100 K). Low laser energies were utilized, and checks were made to ensure that the laser-induced fluorescence signals varied linearly with the laser intensity. Glass filters were placed in front of the CCD camera with 50% transmission cutoffs at 305 and 385 nm. These filters attenuate elastically scattered light from the soot particles and transmit the (0,0) and (1,1) emission bands of OH·. When the laser wavelength was tuned off this OH· rotational line, the OH· fluorescence signal disappeared. Thus, the contribution due to the laser-induced fluorescence signal from OH· could be distinguished easily from that due to the soot scattering [26]. In most images the polarization of the UV light was horizontal relative to the detection axis, which minimized Rayleigh scattering from the soot particles in the direction of the detector. Broadband laser-induced fluorescence was also observed but is much weaker than the OH· fluorescence and the soot scattering signals in the images presented here. This broadband fluorescence has been reported in many earlier studies, including our experiments on Wolfhard–Parker and axisymmetric burners [18, 20, 26], and has been attributed to polycyclic aromatic hydrocarbons (PAH) [75].

The images shown are all single laser shot results, wherein the pixels have been binned by three in each direction, condensing a 576 × 384 format into a 192 × 128 array. With 3.8:1 imaging optics, each frame covers an image area of 32 × 48 mm with an effective spatial resolution of 250 μm/data point in both directions. This resolution is sufficient to characterize the high-temperature reaction zone; for example, our OH· profiles measured on the

[1] Certain commercial equipment is identified herein in order to adequately specify the experimental procedure. Such identification does not imply recommendation by the National Institute of Standards and Technology, nor does it imply that this equipment is the best available for the purpose.

Wolfhard-Parker burner exhibit a full width at half maximum of 1.3 mm [20] for low strain rate conditions [25]. Corrections have been made for background dark counts and scattered light, pixel-to-pixel UV sensitivity (flatfield), and the laser sheet intensity distribution. The flatfield correction was performed using a standard tungsten lamp with a UV diffuser, which produced a uniform light intensity over a circular area of 20 cm^2. Laser-induced fluorescence from dilute BBQ laser dye in methanol was monitored before and after each series of images in order to correct for the variation of the laser sheet intensity in the axial direction. Corrections for the shot-to-shot energy variation of the UV beam ($\leq \pm 20\%$) have not been made for most of the images. This correction has been included for selected images used to quantify the enhanced soot scattering signals observed in the time-varying flames (see next section). Future work will incorporate a separate measurement of both the laser energy and its spatial distribution for each laser shot [68, 69].

RESULTS AND DISCUSSION

Figure 2 presents the OH· laser-induced fluorescence and soot scattering images for a steady-state, laminar CH_4/air flame. Results are shown for both horizontal and vertical polarizations of the incident UV beam with respect to the detection axis. While the OH· fluorescence signal is unpolarized for any state of polarization of the incident light at atmospheric pressure conditions, the elastic scattering from the soot particles is much stronger for vertically polarized incident radiation. Quantitative OH· profiles have been obtained in an earlier investigation of this flame [26] by calibrating the OH· fluorescence signals to absorption data obtained in a CH_4/air diffusion flame burning on a Wolfhard-Parker burner [20]. At a height of 7 mm above the axisymmetric burner the peak OH· concentration is $1.6 \times 10^{16}/cm^3$. For the imaging measurements no corrections have been made for the laser pulse energy and the local quenching rates. Thus, the OH· fluorescence signal serves as a convenient, qualitative marker of the high-temperature reaction zone.

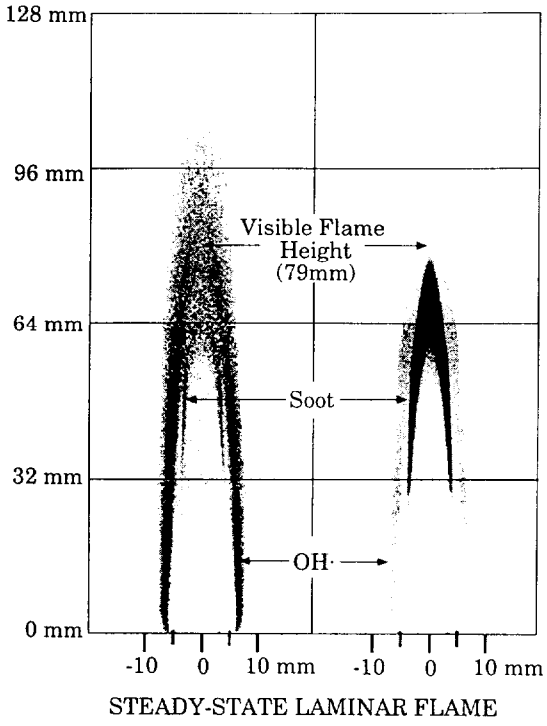

Fig. 2. OH· laser-induced fluorescence and soot scattering images in a steady-state laminar CH_4/air diffusion flame using horizontally polarized incident light (left) and vertically polarized incident light (right). In each case four separate single-shot images have been recorded at different heights above the burner. Note that the gain on the CCD camera was reduced for the latter series, making the OH· fluorescence signals appear weaker. The wavelength of the UV light is 283.55 nm, and the visible flame height is 79 mm above the fuel tube exit, which is located 1 mm above the bottom of the first frame.

Figure 3 shows the results obtained in time-varying flames with the same mean fuel flow velocity (7.9 cm/s) as in the steady-state flame. Two series of images have been obtained at different forcing conditions for ten phase angles as a function of height above the burner. At all times the high-temperature reaction zone appears as a continuous outer envelope, as denoted by the OH· laser-induced fluorescence signals. As the flame height increases and the flame tip is pinched off, soot scattering signals appear in interior, rich regions and become very large. The two series illustrate the effects of different forcing amplitudes upon the interaction of the counter-rotating vortices (in the plane of the laser sheet) with the high-temperature reaction zones and the soot field.

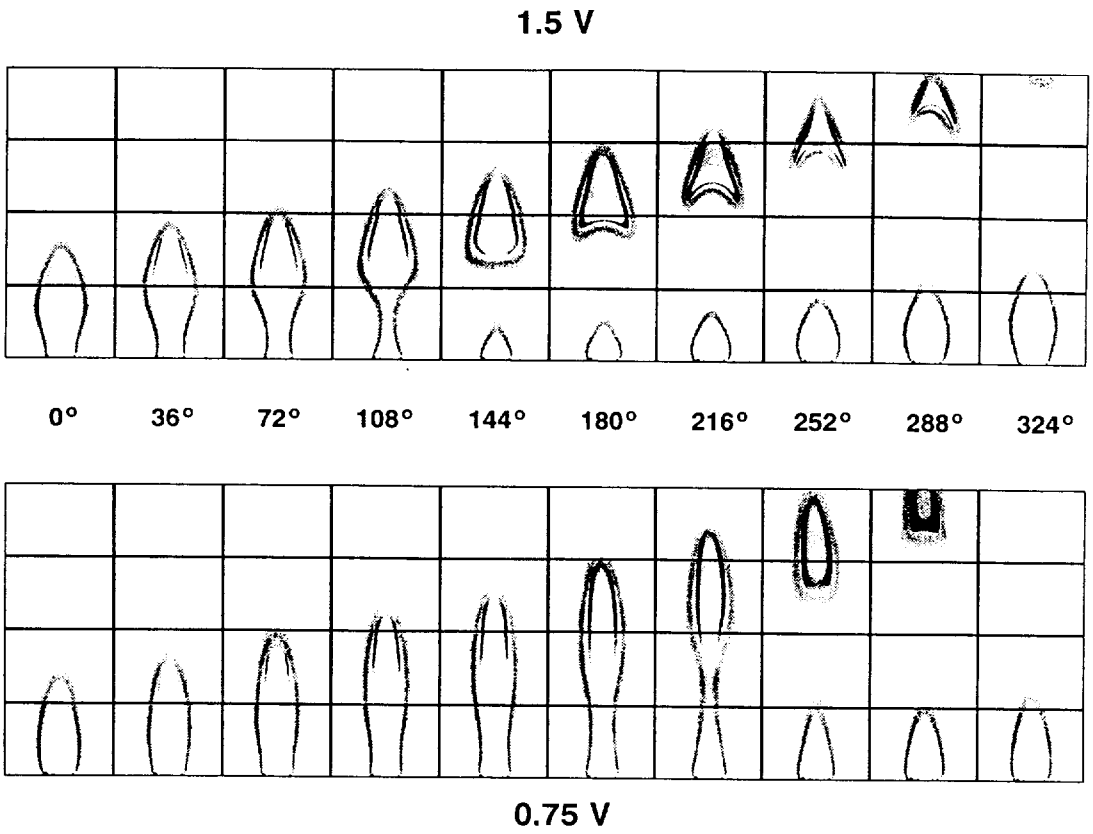

Fig. 3. OH· laser-induced fluorescence and soot scattering images in a time-varying laminar CH_4/air diffusion flame using horizontally polarized incident light at 283.55 nm. Ten phase angles are shown, corresponding to a time interval of 10 ms. The excitation voltage on the loudspeaker is 1.5 V peak-to-peak (top) and 0.75 V (bottom). At each phase angle, four separate single-shot images have been recorded at different heights above the burner. The zero phase angle for each series is arbitrary.

At the higher amplitude the flame tip is clipped off more quickly and is broader, that is, the OH· fluorescence is observed at larger radial positions than for the less vigorous forcing condition. If the acoustic forcing is eliminated and the air co-flow velocity is reduced to ambient conditions, a naturally flickering flame is produced which exhibits vigorous tip clipping images similar to the forced flame with a 1.5-V excitation amplitude. In all cases studied thus far the soot is ultimately oxidized completely, and the methane flames are nonsmoking.

The striking result in comparing the steady-state and time-varying images is the observation that the soot scattering signals in the time-varying flames are greatly enhanced relative to the steady-state, laminar flame burning at the same mean fuel flow velocity (compare the horizontal polarization results in Fig. 2 and Fig. 3). In order to quantify this enhancement, selected images have been corrected for both the laser pulse energy and its spatial distribution. For a highly sooting condition in the time-varying flame, for example the 0.75-V excitation amplitude at a phase angle of 216° (see Fig. 3), the largest observed soot signal at a point is 7–8 times larger than in the steady-state laminar flame using horizontal polarization of the UV beam. Similar enhancements in the scattering signals are observed for vertically polarized light. Figure 4 compares the soot scattering signals integrated along the flame radius as a function of axial location. For this presentation the scattering signals along each row of pixels have been binned together. The maximum soot signal along any row as

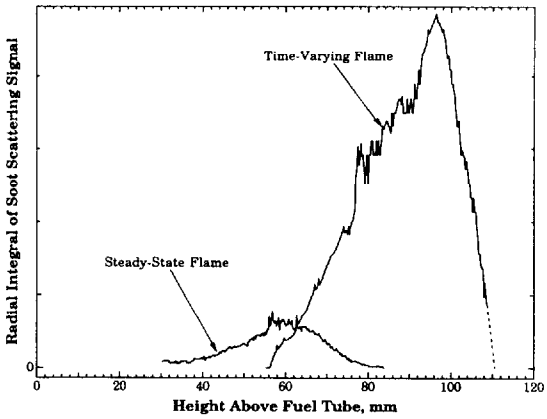

Fig. 4. Integrated soot scattering signals along the flame radius as a function of axial location in the steady-state, laminar CH_4/air flame and the time-varying flame are shown on a relative scale. For the latter the phase angle of 216° has been selected at an excitation amplitude of 0.75 V (see Fig. 3). The polarization of the incident laser beam is horizontal with respect to the detection axis.

well as the integrated soot signal in the plane of the UV laser sheet (as represented by the areas under the curves in Fig. 4) for the time-varying flame at this instant in its evolution are also ≈ 8 times larger than the steady-state values. The enhancement over the entire three-dimensional extent of the time-varying versus steady-state conditions is even greater, approximately a factor of 20, since the radial extent of the soot region is larger in the time-varying flame. If one averages the soot scattering signals over all ten phase angles shown in Fig. 3 (the lower set of uncalibrated images with 0.75-V excitation), rather than selecting one particular time as in Fig. 4, then the enhancement over the entire flame is approximately 10 times that observed in the steady-state flame.

Figure 5 presents a series of images as a function of the peak-to-peak voltage amplitude of the loudspeaker driving voltage. The phase angle of the sine-wave excitation is the same at all voltages and has been chosen to be near the tip-clipping condition in the time-varying flames. For the lowest amplitude excitation (0.2 V), the OH· fluorescence signal shows a small bulge; the tip of the flame has not been pinched off and there is no enhanced soot scattering evident. However, once the shear-induced vortex generation becomes sufficiently vigorous to break off the tip of the flame, much larger soot scattering signals are observed. As the excitation amplitude is increased, the tip clipping occurs earlier and the OH· fluorescence and soot scattering signals show that the pocket of burning gas becomes broader in the radial direction. The effect of the acoustic perturbation of the methane flow upon the flame structure is dramatic. It will be interesting to examine how this perturbation of the fuel flow leads to the observed flickering

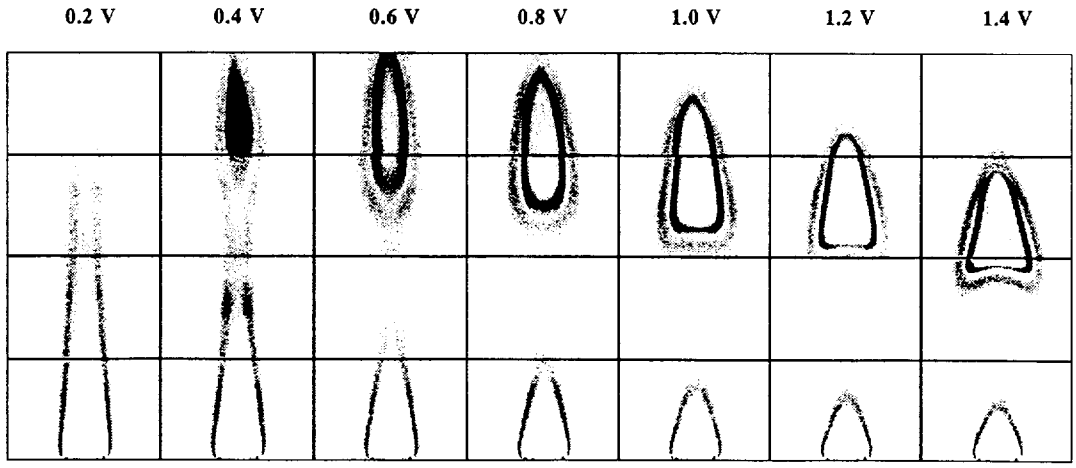

Fig. 5. OH· laser-induced fluorescence and soot scattering images as a function of forcing amplitude in a time-varying laminar CH_4/air diffusion flame. Each set of images has been obtained at the same phase angle and is labeled by the peak-to-peak voltage of the sine wave applied to the loudspeaker. The incident light at 283.55 nm is horizontally polarized with respect to the detection axis.

behavior. Once the tip of the flame is clipped, the local strain rate within the resulting flamelet is expected to be small (i.e., small-velocity derivatives [48]) while the local scalar dissipation rates (mixture fraction gradients) can be quite large.

It is tempting to attribute the greatly increased soot scattering signals in the time-varying flames to a correspondingly large enhancement in the soot volume fraction. However, in the Rayleigh limit of particle sizes that are small relative to the wavelength of the incident radiation, the soot scattering signals are proportional to the sixth power of the particle diameter, whereas the soot volume fraction increases only as the cube of the diameter [72]. Thus, the soot scattering signals are especially sensitive to the particle size distribution and are expected to scale roughly as the square of the soot volume fraction, assuming that the particle number density remains unchanged. It is also conceivable that coalescence and agglomeration could lead to larger particles, and thus enhanced soot scattering signals, without a significant change in the overall soot volume fraction. We are currently making extinction measurements in order to provide complementary information on the local soot volume fraction in the time-varying flames. Extinction may also arise from molecular absorption [75], which will affect the comparison between the steady-state and time-varying flames if the relative contributions of molecular and soot absorption depend upon the local combustion conditions. Additional measurements, such as laser-induced fluorescence of polycyclic aromatic hydrocarbons [26, 75], will be needed to elucidate the contributions of molecular species and soot particles to our laser scattering and extinction measurements.

Methane is an inherently weakly sooting fuel. The large enhancement in the soot scattering signals observed in the time-varying methane flames may be smaller for more heavily sooting fuels. For example, ethylene–air diffusion flames contain much higher soot loadings than CH_4/air flames [2], with up to 15% of the fuel carbon being converted to soot particles in a steady-state flame near the smoke point. If a nonsmoking ethylene flame is acoustically forced into a flickering mode, it produces voluminous smoke. Enhanced soot production in the time-varying flames may lead to greater radiation losses and result in lower soot oxidation rates. However, since the steady-state ethylene–air flame already contains significant soot concentrations, the relative instantaneous *enhancement* of soot production may be smaller than in the time-varying CH_4/air flames.

The principle questions which emerge from our results are what combustion conditions lead to the observed enhancement in the soot scattering signals and to what extent does the soot volume fraction change in the time-varying, laminar CH_4/air flames? Time-varying flames allow investigation of a much wider range of chemistry/flowfield interactions than can be examined under steady-state conditions. This more complex coupling effectively samples different regimes of temperature, mixture fraction, residence time, and strain and scalar dissipation rates than are observed in the steady laminar flames. In order to develop successful soot models for turbulent combustion conditions, the wide range of local conditions under which soot can be produced and destroyed must be accounted for. Using experimental results obtained solely in steady-state, laminar flames it may not be possible to develop comprehensive and representative parametric descriptions that include the correct size distribution of the soot particles. Universal state relationships have not been obtained for species [18] and soot concentrations [4, 76, 77] that vary strongly with residence time. Therefore, such relationships [14–17] are not likely to hold for soot volume fractions in time-varying, diffusion flames. Could the soot production rate maps of Kent and Honnery, which characterize the influence of the temperature, mixture fraction, and residence time upon soot production in steady-state flames [78–80], account for our observations? Once the influence of these parameters as well as the local strain rate upon soot production and oxidation are determined in time-varying flames, the results will serve as critical tests of soot models developed from steady-state flame measurements.

The tip-clipping phenomenon that leads to enhanced soot scattering and likely increased soot production may be important for smoke

and CO emission from turbulent hydrocarbon flames. For fuels that produce more soot than methane, any increase in the soot concentration within the flame will result in larger radiation losses and decreased oxidation rates. With respect to radiation, a number of studies have noted and measured time-varying radiation properties of flickering flames [50, 81–85]. However, thus far no systematic comparison to radiation fluxes from steady-state flames has been made.

Recent numerical modeling studies have yielded good predictions of the time and spatial evolution of buoyant jet diffusion flames [55–57, 86, 87]. Davis has successfully characterized the large scale buoyancy-induced structures observed by Chen, Roquemore, and coworkers [55–57], while Kaplan and Oran have incorporated a soot model into their flickering flame calculations [86, 87]. These modeling efforts should provide useful guidance in determining the properties of the temperature, velocity, and mixture fraction fields in flame regions where soot production rates are large. This combination of experiment and modeling will provide much needed insight into the local residence time, stoichiometry, and temperature conditions, as well as the influence of the strain and scalar dissipation rates upon the chemical processes which lead to soot formation.

CONCLUSIONS

Planar imaging measurements of OH· laser-induced fluorescence and elastic scattering from soot particles in CH_4/air diffusion flames reveal that the soot scattering signals increase dramatically when these flames exhibit tip-clipping flickering instabilities, compared with steady-state laminar conditions. By using acoustic excitation of the fuel flow velocity, the time evolution of the flickering phenomena has been phase locked to our pulsed laser system operating at 10.13 Hz. This experimental arrangement is especially well suited for systematic examination of the influence of vortex/ flame sheet interactions upon chemical processes in hydrocarbon diffusion flames. Fluorescence imaging of a wide variety of additional important combustion species can be readily accomplished in these flames, including O atoms [21], CH· [23], CO [22, 88], NO· [89], and formaldehyde [24].

We thank Richard Joklik for providing us with a plenum design for the acoustic locking experiments, Chris Cromer for loaning us the standard tungsten lamp, and Anthony Hamins, George Mulholland, and Chris Shaddix for stimulating discussions on flickering diffusion flames and soot production processes.

REFERENCES

1. Glassman, I., *Twenty-Second Symposium (International) on Combustion,* The Combustion Institute, Pittsburgh, 1988, p. 295 and references therein.
2. Santoro, R. J., Yeh, T. T., Horvath, J. J., and Semerjian, H. G., *Combust. Sci. Technol.* 53:89–115 (1987).
3. Dobbins, R. A., Santoro, R. J., and Semerjian, H. G., *Twenty-Third Symposium (International) on Combustion,* The Combustion Institute, Pittsburgh, 1990, p. 1525.
4. Moss, J. B., Stewart, C. D., and Syed, K. J., *Twenty-Second Symposium (International) on Combustion,* The Combustion Institute, Pittsburgh, 1988, p. 413.
5. Syed, K. J., Stewart, C. D., and Moss, J. B., *Twenty-Third Symposium (International) on Combustion,* The Combustion Institute, Pittsburgh, 1990, p. 1533.
6. Stewart, C. D., Syed, K. J., and Moss, J. B., *Combust. Sci. Technol.* 75:211–226 (1991).
7. Kennedy, I. M., Kollmann, W., and Chen, J.-Y., *Combust. Flame* 81:73–85 (1990).
8. Kennedy, I. M., Kollmann, W., and Chen, J.-Y., *AIAA J.* 29:1452–1457 (1991).
9. Leung, K. M., Lindstedt, R. P., and Jones, W. P., *Combust. Flame* 87:289–305 (1991).
10. Lindstedt, R. P., to appear in *Mechanisms and Models of Soot Formation,* Lecture Notes in Physics, Springer-Verlag, 1993.
11. Honnery, D. R., Tappe, M., and Kent, J. H., *Combust. Sci. Technol.* 83:305–321 (1992).
12. Kent, J. H., and Honnery, D. R., to appear in *Mechanisms and Models of Soot Formation,* Lecture Notes in Physics, Springer-Verlag, 1993.
13. Honnery, D. R., and Kent, J. H., *Twenty-Fourth Symposium (International) on Combustion,* The Combustion Institute, Pittsburgh, 1992, p. 1041.
14. Gore, J. P., and Faeth, G. M., *Twenty-First Symposium (International) on Combustion,* The Combustion Institute, Pittsburgh, 1986, p. 1521.
15. Gore, J. P., and Faeth, G. M., *J. Heat Transf.* 110:173–181 (1988).
16. Sivathanu, Y. R., Gore, J. P., and Faeth, G. M., *Combust. Flame* 73:315–329 (1988).
17. Sivathanu, Y. R., and Faeth, G. M., *Combust. Flame* 81:133–149 (1990).
18. Smyth, K. C., Miller, J. H., Dorfman, R. C., Mallard,

W. G., and Santoro, R. J., *Combust. Flame* 62:157–181 (1985).
19. Smyth, K. C., and Taylor, P. H., *Chem. Phys. Lett.* 122:518–522 (1985).
20. Smyth, K. C., Tjossem, P. J. H., Hamins, A., and Miller, J. H., *Combust. Flame* 79:366–380 (1990).
21. Smyth, K. C., and Tjossem, P. J. H., *Twenty-Third Symposium (International) on Combustion,* The Combustion Institute, Pittsburgh, 1990, p. 1829.
22. Smyth, K. C., and Tjossem, P. J. H., *Appl. Opt.* 29:4891–4898 (1990).
23. Norton, T. S., and Smyth, K. C., *Combust. Sci. Technol.* 76:1–20 (1991).
24. Harrington, J. E., and Smyth, K. C., *Chem. Phys. Lett.* 202:196–202 (1993).
25. Norton, T. S., Smyth, K. C., Miller, J. H., and Smooke, M. D., *Combust. Sci. Technol.* 90:1–34 (1993).
26. Puri, R., Moser, M., Santoro, R. J., and Smyth, K. C., *Twenty-Fourth Symposium (International) on Combustion,* The Combustion Institute, Pittsburgh, 1992, p. 1015.
27. Smooke, M. D., Ed., *Reduced Kinetic Mechanisms and Asymptotic Approximations for Methane–Air Flames,* Lecture Notes in Physics, Vol. 384, Springer-Verlag, Berlin, 1991.
28. Hamins, A., Yang, J. C., and Kashiwagi, T., *Twenty-Fourth Symposium (International) on Combustion,* The Combustion Institute, Pittsburgh, 1992, p. 1695 and references therein.
29. Buckmaster, J., and Peters, N., *Twenty-First Symposium (International) on Combustion,* The Combustion Institute, Pittsburgh, 1986, p. 1829.
30. Coats, C. M., and Zhao, H., *Twenty-Second Symposium (International) on Combustion,* The Combustion Institute, Pittsburgh, 1988, p. 685.
31. Zukoski, E. E., Cetegen, B. M., and Kubota, T., *Twentieth Symposium (International) on Combustion,* The Combustion Institute, Pittsburgh, 1984, p. 361.
32. Cetegen, B. M., and Ahmed, T. A., *Combust. Flame* 93:157–184 (1993).
33. Kimura, I., *Tenth Symposium (International) on Combustion,* The Combustion Institute, Pittsburgh, 1965, p. 1295.
34. Pearson, I. G., Cabelli, A., Shepherd, I. C., and Hamilton, N. B., *10th Australasian Fluid Mechanics Conference* I, 5.27–5.30 (1989).
35. Chamberlin, D. S., and Rose, A., *Proceedings of the First Symposium on Combustion,* The Combustion Institute, Pittsburgh, 1928, p. 27.
36. Wohl, K., Kapp, N. M., and Gazley, C., *Third Symposium on Combustion, Flame, and Explosion Phenomena,* Williams and Wilkins Co., Baltimore, 1949, p. 3.
37. Barr, J., *Fourth Symposium on Combustion, Flame, and Explosion Phenomena,* Williams and Wilkins Co., Baltimore, 1953, p. 765.
38. Maklakov, A. I., *Zhur. Fiz. Khim.* 30:708 (1956).
39. Toong, T.-Y., Salant, R. F., Stopford, J. M., and Anderson, G. Y., *Tenth Symposium (International) on Combustion,* The Combustion Institute, Pittsburgh, 1965, p. 1301.
40. Durão, D. F. G., and Whitelaw, J. H., *Proc. R. Soc. London. A* 338:479–501 (1974).
41. Grant, A. J., and Jones, J. M., *Combust. Flame* 25:153–160 (1975).
42. Ballantyne, A., and Bray, K. N. C., *Sixteenth Symposium (International) on Combustion,* The Combustion Institute, Pittsburgh, 1977, p. 777.
43. McCaffrey, B. J., National Bureau of Standards Internal Report NBSIR 79-1910 (1979).
44. Becker, H. A., and Liang, D., *Combust. Flame* 52:247–256 (1983).
45. Eickhoff, H., and Winandy, A., *Combust. Flame* 60:99–101 (1985).
46. Miake-Lye, R. C., and Toner, S. J., *Combust. Flame* 67:9–26 (1987).
47. Strawa, A. W., and Cantwell, B. J., *Phys. Fluids* 28:2317–2320 (1985).
48. Lewis, G. S., Cantwell, B. J., Vandsburger, U., and Bowman, C. T., *Twenty-Second Symposium (International) on Combustion,* The Combustion Institute, Pittsburgh, 1988, p. 515.
49. Vandsburger, U., Seitzman, J. M., and Hanson, R. K., *Combust. Sci. Technol.* 59:455–461 (1988).
50. Strawa, A. W., and Cantwell, B. J., *J. Fluid Mech.* 200:309–336 (1989).
51. Mahalingam, S., Cantwell, B. J., and Ferziger, J. H., *Phys. Fluids A* 2:720–728 (1990).
52. Chen, L.-D., and Roquemore, W. M., *Combust. Flame* 66:81–86 (1986).
53. Roquemore, W. M., Chen, L.-D., Goss, L. P., and Lynn, W. F., in *Turbulent Reacting Flows* (R. Borghi and S. N. B. Murthy, Eds.), Springer-Verlag, Berlin, 1989, pp. 49–63.
54. Chen, L.-D., Seaba, J. P., Roquemore, W. M., and Goss, L. P., *Twenty-Second Symposium (International) on Combustion,* The Combustion Institute, Pittsburgh, 1988, p. 677.
55. Davis, R. W., Moore, E. F., Santoro, R. J., and Ness, J. R., *Combust. Sci. Technol.* 73:625–635 (1990).
56. Davis, R. W., Moore, E. F., Roquemore, W. M., Chen, L.-D., Vilimpoc, V., and Goss, L. P., *Combust. Flame* 83:263–270 (1991).
57. Chen, L.-D., Vilimpoc, V., Goss, L. P., Davis, R. W., Moore, E. F., and Roquemore, W. M., *Twenty-Fourth Symposium (International) on Combustion,* The Combustion Institute, Pittsburgh, 1992, p. 303.
58. Pearson, I. G., and Proctor, D., *Experimental Heat Transfer, Fluid Mechanics, and Thermodynamics,* 1991, pp. 316–322.
59. Cabelli, A., Pearson, I. G., Shepherd, I. C., and Hamilton, N. B., submitted to *J. Heat Transf.*
60. Dobbins, R. A., and Subramaniasivam, H., *Mechanisms and Models of Soot Formation,* Lecture Notes in Physics, Springer-Verlag, Berlin, in press.
61. Gutmark, E., Parr, T. P., Parr, D. M., and Schadow, K. C., *Twenty-Second Symposium (International) on Combustion,* The Combustion Institute, Pittsburgh, 1988, p. 523.
62. Gutmark, E., Parr, T. P., Parr, D. M., and Schadow, K. C., *J. Heat Transf.* 111:148–155 (1989).

63. Gutmark, E., Parr, T. P., Hanson-Parr, D. M., and Schadow, K. C., *Combust. Sci. Technol.* 66:107–126 (1989).
64. Gutmark, E., Parr, T. P., Hanson-Parr, D. M., and Schadow, K. C., Western States Section/The Combustion Institute, 1992 Fall Meeting, Paper No. 92-70.
65. Lovett, J. A., and Turns, S. R., *AIAA J.* 28:38–46 (1990).
66. Lovett, J. A., and Turns, S. R., *Combust. Sci. Technol.*, in press.
67. Kim, T. K., Park, J., and Shin, H. D., *Combust. Sci. Technol.* 89:83–100 (1993).
68. Cattolica, R. J., and Vosen, S. R., *Combust. Sci. Technol.* 48:77–87 (1986).
69. Cattolica, R. J., and Vosen, S. R., *Twentieth Symposium (International) on Combustion*, The Combustion Institute, Pittsburgh, 1984, p. 1273.
70. Jarosinski, J., Lee, J. H. S., and Knystautas, R., *Twenty-Second Symposium (International) on Combustion*, The Combustion Institute, Pittsburgh, 1988, p. 505.
71. Roberts, W. L., Driscoll, J. F., Drake, M. C., and Ratcliffe, J. W., *Twenty-Fourth Symposium (International) on Combustion*, The Combustion Institute, Pittsburgh, 1992, p. 169.
72. Santoro, R. J., Semerjian, H. G., and Dobbins, R. A., *Combust. Flame* 51:203–218 (1983).
73. Collis, D. C., and Williams, M. J., *J. Fluid Mech.* 6:357–384 (1959).
74. Hatton, A. P., James, D. D., and Swire, H. W., *J. Fluid Mech.* 42:17–31 (1970).
75. Miller, J. H., Mallard, W. G., and Smyth, K. C., *Combust. Flame* 47:205–214 (1982) and references therein.
76. Kent, J. H., and Honnery, D., *Combust. Sci. Technol.* 54:383–397 (1987).
77. Sivathanu, Y. R., and Gore, J. P., Central and Eastern States Meeting of the Combustion Institute (New Orleans, March, 1993), paper #123.
78. Kent, J. H., and Honnery, D. R., *Combust. Flame* 79:287–298 (1990).
79. Honnery, D. R., and Kent, J. H., *Combust. Flame* 82:426–434 (1990).
80. Kent, J. H., and Honnery, D. R., *Combust. Sci. Technol.* 75:167–177 (1991).
81. McCamy, C. S., *J. Res. Natl. Bur. Stand.* 56:293–299 (1956).
82. Portscht, R., *Combust. Sci. Technol.* 10:73–84 (1975).
83. Hertzberg, M., Cashdollar, K., Litton, C., and Burgess, D., U.S. Bureau of Mines, Report Number 8263 (1978).
84. Detriche, Ph., and Lanore, J. C., *Fire Technol.* 16:204–211 (1980).
85. Schönbucher, A., Goeck, D., Kettler, A., Krattenmacher, D., and Schiess, N., *Twenty-First Symposium (International) on Combustion*, The Combustion Institute, Pittsburgh, 1986, p. 93.
86. Kaplan, C. R., Baek, S. W., and Oran, E. S., AIAA Paper #93-0109 (1993).
87. Kaplan, C. R., Baek, S. W., Oran, E. S., and Ellzey, J. L., *Combust. Flame*, in press.
88. Tjossem, P. J. H., and Smyth, K. C., *J. Chem. Phys.* 91:2041–2048 (1989).
89. Carter, C. D., and Barlow, R. S., Western States Section/The Combustion Institute, 1992 Spring Meeting, Paper No. 92-47.

Received 11 February 1993; revised 8 June 1993